

Charge Transfer with a Spin. II: A Framework for Diabatization which Localizes Charge and Spin

Alok Kumar,^{†,‡} Zhen Tao,[¶] Zuxin Jin,[†] Joseph E. Subotnik,[‡] and Tian Qiu^{*,‡}

[†]*Department of Chemistry, University of Pennsylvania, Philadelphia, Pennsylvania, 19104, USA*

[‡]*Department of Chemistry, Princeton University, Princeton, New Jersey, 08540, USA*

[¶]*Department of Chemistry, University of Rhode Island, Kingston, Rhode Island, 02881, USA*

E-mail: tianq@princeton.edu

Abstract

We investigate a diabatization procedure that localizes charges (in real space) and localizes spins (in spin space) for open-shell systems that exhibit charge transfer in the presence of spin-orbit coupling. The procedure is applied to a two-state crossing between pairs of Kramers-restricted doublet states (which can also be considered effectively a four-state crossing). To generate the relevant electronic states, we employ the recently developed electron/hole-transfer Dynamically-weighted State-Averaged Constrained CASSCF (eDSC/hDSC) method that treats systems with an odd number of electrons. To generate the relevant diabatic states, we employ a two-step optimization over complex-unitary rotations that sequentially maximizes dipole and spin moments through iterative Jacobi sweeps; the resulting update rules are effectively equivalent to those of approximate joint diagonalization (AJD) applied to charge and spin. The

method converges rapidly and yields smooth diabatic potential energy surfaces that preserve dipole and spin properties (e.g., a slowly varying pseudospin texture) along the reaction coordinate while maintaining time-reversal symmetry.

1 Introduction

Charge-transfer (CT) processes play a central role in a wide range of phenomena from photosynthetic electron transfer^{1–3} and molecular photovoltaics^{4,5} to spin–orbit–coupled phenomena in transition-metal complexes^{6,7} and chiral molecular systems.^{8–10} In many of these systems, multiple electronic states interact strongly with nuclear motion,^{11–13} and in open-shell systems, additional coupling between spin and orbital angular momentum introduces nontrivial spin dynamics. These couplings make the adiabatic representation, though convenient for electronic structure calculations, ill-suited for describing charge localization and nonadiabatic population transfer.^{14,15} Accurate modeling of electron transfer processes often demands the construction of diabatic states, which simplify the description of state-to-state couplings and charge localization.

Constructing diabatic states that remain physically meaningful in the presence of spin–orbit coupling (SOC) presents two distinct challenges, as SOC breaks spin conservation and entangles spatial and spin degrees of freedom. First, traditional diabatization schemes, including Boys/GMH localization,^{16–19} Edmiston–Ruedenberg,²⁰ fragment charge diabatization and fragment energy diabatization,^{21–25} or block-diagonalization^{26,27} approaches, are designed for spin-free adiabatic states and therefore cannot handle the degenerate (or nearly degenerate) complex-valued spinors required to describe open-shell systems with strong SOC. Interestingly, fragment spin difference²⁸ (which is designed for spin-processes) does not distinguish between different spin states of a given spin manifold. Previous studies of multistate density functional theory (MSDFT) have mainly focused on spin-multiplet energy splittings,^{29–31} with limited treatment of how the spin character evolves with molecular geometry. Second, although SOC is commonly introduced as a fixed perturbation on spin-free electronic states,

in reality its magnitude and phase evolve with nuclear geometry, reflecting the continuous mixing of spin and orbital angular momenta,^{32–34} necessitating extreme attention to phases and degeneracies (with many crossings possible). One previous approach to diabatization in the presence of SOC (by Zeng³⁵) sought to construct and follow smooth SOC matrix elements along nuclear distortions by following the character of the one-electron orbitals, as pioneered by Atchity and Ruedenberg³⁶) and Truhlar and co-workers,^{37,38} and rotating to a given reference set of states. This approach is viable, but will be tedious for large molecules, especially if we include SOC before diagonalization (and thus must be much more careful when tracking diabatic states).

In practice, if our goal is to develop meaningful diabatic states in the context of charge transfer, our intuition is that the most straightforward diabatization protocol requires that we localize not only charge but also spin. Localizing spin (in spin space) means choosing diabatic states whose spin-quantization axis varies smoothly along the reaction coordinate, rather than twisting arbitrarily with geometry. A slowly and smoothly varying spin axis ensures that changes in the spin expectation values reflect genuine spin–orbit–driven physics, rather than arbitrary choices of gauge, especially within a degenerate manifold. With this intuition in mind, below we present a unified diabatization framework that localizes both charge and spin through unitary rotations, all in the presence of SOC. Our procedure builds upon Boys localization conceptually, originally formulated for orbitals^{17,20} and later extended to many-electronic states,¹⁹ and generalizes the latter to include spin operators. The first paper (which we will refer to as Paper 1) of this two part articles has outlined how to obtain adiabatic states for charge transfer in presence of SOC. In this (second) paper, we develop a diabatization scheme, apply it to the previously mentioned adiabatic states, and demonstrate that such a scheme yields charge and spin localized diabatic states with smooth energies and spin texture.

An outline of this article is as follows. In Sec. 2, we review the adiabatic-to-diabatic basis transformation and motivate why molecules with an odd number of electrons are an

interesting system to study spin diabatization. In Sec. 3, we present our two-step, Boys-localization inspired, diabatization procedure in the context of a four state problem, with two spatial states and two spin, corresponding to a spin-dependent electron transfer. We also present numerical results demonstrating the diabatic energy surfaces and spin contamination in Sec. 4. In Sec. 5, we discuss the subtle but significant difference between spin symmetry and time-reversal symmetry and what that difference means in context of spin contamination. Finally, in Sec. 6, we conclude and highlight the future dynamical implications of a slowly, smoothly non-adiabatic smooth diabatic basis as far as understanding radical electron transfer.

2 Method

2.1 Adiabatic and diabatic basis

Within the Born–Oppenheimer approximation, the full molecular Hamiltonian can be written as

$$\hat{H}(\mathbf{r}, \mathbf{R}) = \hat{T}_{\text{nuc}} + \hat{H}_{\text{el}}(\mathbf{r}; \mathbf{R}), \quad (1)$$

where \mathbf{r} and \mathbf{R} denote electronic and nuclear coordinates, respectively, \hat{T}_{nuc} is the nuclear kinetic energy operator, and $\hat{H}_{\text{el}}(\mathbf{r}; \mathbf{R})$ is the electronic Hamiltonian for clamped nuclei. For each fixed nuclear geometry, the adiabatic electronic states $|\psi_k(\mathbf{R})\rangle$ are defined as the eigenfunctions of the electronic Hamiltonian,

$$\hat{H}_{\text{el}} |\psi_k\rangle = E_k |\psi_k\rangle, \quad (2)$$

and the associated eigenvalues E_k define the adiabatic potential energy surface. These adiabatic states form an orthonormal basis at each geometry and are the natural output from any electronic-structure calculation. However, as is well-known,^{38–40} these adiabatic states

usually do not coincide with the chemically intuitive electronic configurations that one would like to follow along a reaction coordinate. Moreover, in the presence of external degrees of freedom like nuclear vibrations or solvent environment, these adiabatic eigenstates of the isolated system may not be stationary states.⁴¹ Lastly, in the vicinity of avoided crossings, the charge distribution (and thus the dipole moment expectation values) as well as the spin expectation values can vary sharply. For all of these reasons, and in order to model electron transfer à la Marcus theory,⁴² there is a strong reason to consider a different, diabatic electronic basis, which has largely constant electronic character and is stabilized by the environment.

To obtain states that are better aligned with chemical intuition, the standard approach today^{40,43} is to exploit the unitary freedom within a chosen adiabatic manifold $\{|\psi_k\rangle\}$ (of n states) and construct a diabatic basis $\{|\xi_i\rangle\}$ via a geometry-dependent unitary transformation,

$$|\xi_i\rangle = \sum_j^n |\psi_j\rangle U_{ji} \quad (3)$$

where \mathbf{U} is a unitary matrix of size $n \times n$. Above, \mathbf{U} is usually called an adiabatic-to-diabatic transformation.

2.2 Diabatization For Electron Transfer (Without Spin): Boys localization

Let us temporarily ignore electronic spin. When electron transfer happens, we typically need two diabatic states to represent the initial and final states of electron transfer.³⁹ The Boys localization scheme was originally developed for localizing orbitals^{16,44} and was later extended to the localization of many-electron states.^{18,19} We begin with a set of adiabatic states $\{|\psi_k\rangle\}$ and define a unitary rotation matrix \mathbf{U} as in Eq. 3 such that it maximizes the

magnitude of dipole moment difference between diabatic states.

$$f_{\text{Boys}}(\mathbf{U}) = \sum_{i,j} \left| \langle \xi_i | \hat{\mu} | \xi_i \rangle - \langle \xi_j | \hat{\mu} | \xi_j \rangle \right|^2 \quad (4)$$

where $\hat{\mu}$ is the electric dipole operator.

The maximization in Eq. 4 is equivalent to maximizing the sum of the magnitudes of the dipole moments of all the states

$$f_{\text{Boys}}(\mathbf{U}) \equiv \sum_i \left| \langle \xi_i | \hat{\mu} | \xi_i \rangle \right|^2 \quad (5)$$

As evident from Eq. 5, the Boys objective function can be written as a sum of the squares of the diagonals of a collection of dipole matrices ($\boldsymbol{\mu}_x, \boldsymbol{\mu}_y, \boldsymbol{\mu}_z$) in a diabatic basis; maximizing such an objective function is therefore equivalent to seeking a unitary rotation that (approximately) diagonalizes all three matrices. An equivalent viewpoint is to cumulatively minimize the off-diagonal elements, leading to the approximate joint diagonalization (AJD) formulation for a set of Hermitian matrices. Closed-form AJD updates have been developed for complex unitary rotations and successfully used for orbital localization in presence of SOC.^{45,46}

In practice, in order to maximize the function in Eq. 5, one usually follows the approach in Ref. 20. Namely, instead of optimizing the full unitary matrix at once, we perform successive 2×2 rotations within subspaces spanned by pairs of adiabatic states, for which the Boys function can be maximized exactly. Iterating this pairwise optimization over all state pairs and repeating the sweep until changes in the objective are negligible yields a unitary transformation that gives *approximately* diagonal dipole moment matrices. In practice, the procedure above, with so-called “Jacobi sweeps”, usually converge fairly quickly reaching a maximum after only a few sweeps, regardless of the number of charge centers or states.¹⁹ The resulting diabatic states usually have small (though certainly not zero) derivative couplings.⁴⁷

2.3 Odd-electron molecule and Kramers degeneracy

The requirements of a diabatization scheme become more involved in the presence of spin because of Kramers' degeneracy. For a system with an odd number of electrons, a theorem due to Kramers, states that in the absence of external magnetic fields, every energy level is at least doubly degenerate.⁴⁸ These degeneracies arise from the invariance of the Hamiltonian under the anti-linear time-reversal symmetry (TRS) operator \hat{T} . If the Hamiltonian \hat{H} is time-reversal symmetric,

$$[\hat{H}, \hat{T}] = 0, \quad (6)$$

and $|\psi\rangle$ is an eigenstate with energy E , then $\hat{T}|\psi\rangle$ is also an eigenstate with the same energy,

$$\hat{H}|\psi\rangle = E|\psi\rangle \quad \Rightarrow \quad \hat{H}\hat{T}|\psi\rangle = E\hat{T}|\psi\rangle. \quad (7)$$

The two degenerate states are related by the time-reversal operator which satisfies $\hat{T}^2 = -1$. Such a pair, $\{|\psi\rangle, |\bar{\psi}\rangle\}$, forms a *Kramers pair* and obeys

$$\hat{T}|\psi\rangle = |\bar{\psi}\rangle, \quad (8)$$

$$\hat{T}^2|\psi\rangle = -|\psi\rangle, \quad (9)$$

$$\langle\psi|\bar{\psi}\rangle = 0 \quad (10)$$

The states in a Kramers pair span a two-dimensional degenerate subspace. Within this subspace, there is no unique choice of orthonormal basis: any pair of orthonormal linear combinations is equally valid and yields the same energies and other time-reversal-even observables (dipole, spin-orbit coupling etc.). Physically, this internal freedom can be viewed as the freedom to attach a different spin-quantization axis to the doublet. By applying geometry-dependent unitary rotations that mix the two members of a Kramers pair, one leaves the overall spectrum unchanged while continuously changing the direction of the local

spin expectation value. If this freedom is not controlled, the spin along a reaction coordinate is masked by such arbitrary gauge rotations, obscuring a clear interpretation of how spin can couple to nuclear motion.

Vice versa, by enforcing a slowly and smoothly varying spin-quantization axis—for instance, via a spin-localization criterion that minimizes the off-diagonal components of the spin operator within each Kramers pair—we effectively establish a gauge convention. In this gauge, the local spin expectation value for each diabat (which behaves as a pseudospin) varies slowly and smoothly with nuclear geometry and can be interpreted as a well-defined geometric observable. (See Sec. 7.1 for a discussion about SU(2) gauge and pseudospin.) Fig. 1 shows a schematic of a charge transfer process where a molecule (and presumably its environment) undergoes a nuclear rearrangement (vibrations, rotations, etc.) as it goes through curve crossing. Imagine a molecule with N atoms, with $3N$ total degrees of freedom, and $3N-3$ internal degrees of freedom (after removing the center-of mass; see Panel B, where each axis is 3-dimensional). During a rearrangement, in presence of SOC, the spin-quantization axis of Kramers pair can rotate to give a geometry-dependent pseudospin-texture.

3 Diabatization of charge and spin

Let us now imagine we are diabatizing a system with $2N$ electronic states, arranged in Kramers' pairs as described above. Our goal is to construct quasi-diabatic states for charge-transfer systems with SOC that simultaneously satisfy three goals: (i) we must localize the charge, (ii) we must localize the spin, and (iii) we must preserve time-reversal symmetry. Because of the nature of the algorithm discussed above, our proposed diabatization can be defined by focusing one at a time on a given pair of states (to be rotated together).

To that end, consider two adiabatic states, $|\psi_1\rangle$ and $|\psi_2\rangle$ respectively. These are orthonormal eigenstates of the electronic Hamiltonian, and their time-reversed partners can

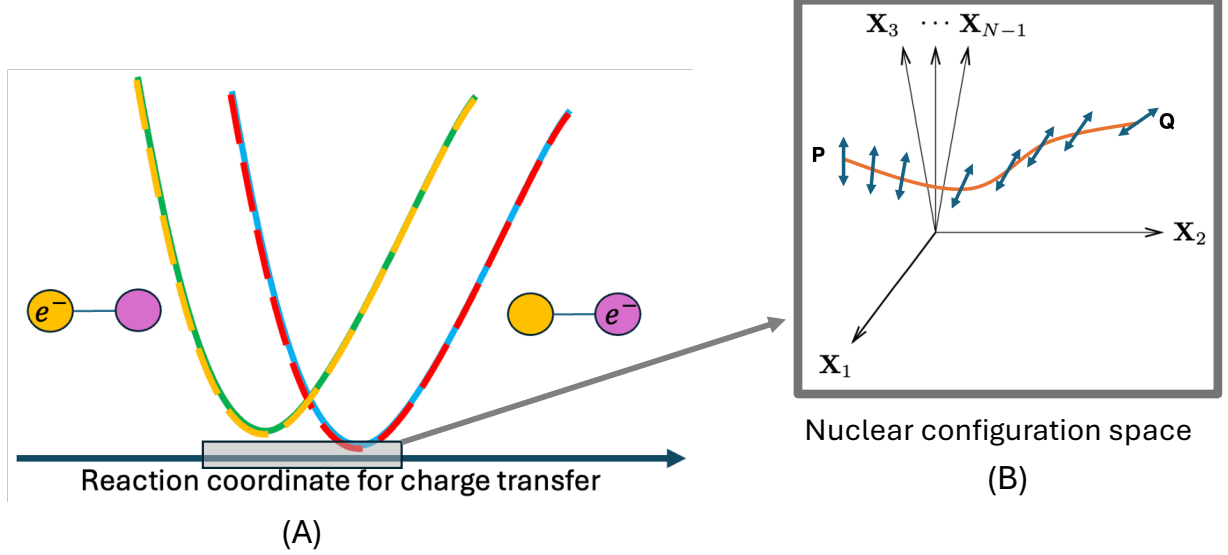


Figure 1: Schematic illustration of charge transfer and pseudospin texture in an odd-electron system. (A) Doubly degenerate diabatic potential energy surfaces corresponding to charge being localized on left (or right fragment) as shown on yellow (magenta) balls. (B) Multi-dimensional nuclear configuration space. A nuclear trajectory from configuration P to Q (orange curve) defines an effective reaction coordinate; along this path, the spin-quantization axis of a Kramers doublet (blue arrows) can rotate, generating a non-trivial pseudospin texture.

be defined as

$$|\bar{\psi}_k\rangle = \hat{T}|\psi_k\rangle, \quad k \in \{1, 2\}. \quad (11)$$

Each Kramers pair $\{|\psi_k\rangle, |\bar{\psi}_k\rangle\}$ forms an orthonormal doublet. Moreover, if $\{|\psi_1\rangle, |\psi_2\rangle\}$ is an orthonormal set, then their respective time-reversed partners $\{|\bar{\psi}_1\rangle, |\bar{\psi}_2\rangle\}$ are also orthonormal, since

$$\langle \bar{\psi}_1 | \bar{\psi}_2 \rangle = \langle \hat{T}\psi_1 | \hat{T}\psi_2 \rangle = (\langle \psi_1 | \psi_2 \rangle)^* \quad (12)$$

Thus the four adiabatic states $\{|\psi_1\rangle, |\psi_2\rangle, |\bar{\psi}_1\rangle, |\bar{\psi}_2\rangle\}$ can be chosen as an orthonormal basis of the relevant 4-dimensional subspace, and the relevant diabatic basis $\{|\xi_1\rangle, |\xi_2\rangle, |\bar{\xi}_1\rangle, |\bar{\xi}_2\rangle\}$ is obtained from the adiabatic basis by a unitary transformation. Since the adiabatic eigen-

states are two-component spinor wavefunctions with complex-valued coefficients (due to the presence of spin-orbit coupling), the adiabatic-to-diabatic transformation matrix \mathbf{U} must be taken as a general complex-valued unitary matrix rather than a purely real orthogonal rotation as in Eq. 4. By restricting \mathbf{U} to the subgroup that preserves the Kramers structure (i.e., acting with $SU(2)$ rotations within each Kramers pair and mixing the two doublets in a TRS-consistent way), we ensure that the diabatic states remain orthonormal and organized into Kramers pairs, while achieving simultaneous charge and spin localization along the reaction coordinate. See section 3.2 for more details about preserving time-reversal symmetry during adiabatic-to-diabatic transformation.

3.1 Optimization functions

We employ a two-step diabatization scheme to achieve simultaneous charge and spin localization. In the first step, we maximize the dipole expectation values, followed by the maximization of the spin expectation values. The two functions being maximized are:

$$\text{Localize dipole:} \quad f_1(\mathbf{U}) = \sum_i \sum_{\alpha=x,y,z} |\langle \xi_i | \hat{\mu}_\alpha | \xi_i \rangle|^2 + |\langle \bar{\xi}_i | \hat{\mu}_\alpha | \bar{\xi}_i \rangle|^2 \quad (13)$$

$$\text{Localize spin:} \quad f_2^i(\mathbf{U}) = \sum_{\alpha=x,y,z} \left| \langle \xi_i | \hat{S}_\alpha | \xi_i \rangle \right|^2 + \left| \langle \bar{\xi}_i | \hat{S}_\alpha | \bar{\xi}_i \rangle \right|^2 \quad (14)$$

where $\hat{\mu}_\alpha$ and \hat{S}_α are the Cartesian dipole moment and spin matrices, respectively. Note that the optimization for localizing dipole is performed over all four states simultaneously (Eq. 13) whereas spin localization (for each charge diabatized state i) is between time reversal pairs only (Eq. 14). We follow an iterative procedure of Jacobi sweeps to find a sequence of optimal rotation matrix \mathbf{U} that maximizes these functions while preserving time-reversal symmetry.

3.2 Jacobi sweeps with Time Reversal Symmetry

In the absence of external magnetic fields or other time-reversal-breaking interactions, the electronic Hamiltonian commutes with the time-reversal operator \hat{T} (Eq. 6). Our diabatization procedure should not artificially break this symmetry. This requirement makes each Jacobi rotation slightly more constrained than in a generic complex Jacobi sweep.

The rotation matrix \mathbf{U} is a complex unitary matrix that transforms the adiabatic basis to the diabatic one. We construct \mathbf{U} as a product of sequential Jacobi rotations, each acting in a low-dimensional subspace spanned by a small number of adiabatic states,

$$\mathbf{U} = \prod_m \mathbf{Q}_m, \quad (15)$$

where each \mathbf{Q}_m differs from the identity only within the selected subspace. At this point, it is useful to distinguish two types of rotations:

(i) Rotations within a single Kramers pair: Spin diabatization. Consider a Kramers doublet (i, \bar{i}) belonging to a given charge-localized state (where $|\bar{i}\rangle = \hat{T}|i\rangle$). We label the states using just the indices for brevity. In the ordered basis (i, \bar{i}) , the corresponding 2×2 block of \mathbf{Q}_m is

$$\mathbf{Q}_m(\gamma, \phi) = \begin{bmatrix} \cos \gamma & -\sin \gamma e^{-i\phi} \\ \sin \gamma e^{i\phi} & \cos \gamma \end{bmatrix}, \quad (16)$$

with all other matrix elements equal to those of the identity. Because $|\bar{i}\rangle = \hat{T}|i\rangle$ and \hat{T} is antiunitary, one can easily show that any such SU(2) rotation automatically preserves the Kramers relation between the two rotated states, i.e. $|\bar{i}'\rangle = \hat{T}|i'\rangle$. In our calculations we perform one such rotation in each charge-localized state.

(ii) **Rotations between two different Kramers pairs: Dipole diabatization.** Dipole localization mixes two distinct Kramers pairs, say (i, \bar{i}) and (j, \bar{j}) . Here time-reversal symmetry requires that we rotate the four states $\{|i\rangle, |j\rangle, |\bar{i}\rangle, |\bar{j}\rangle\}$ together: an arbitrary 2×2 rotation between $|i\rangle$ and $|j\rangle$ must be accompanied by a corresponding rotation between their time-reversal partners $|\bar{i}\rangle$ and $|\bar{j}\rangle$, otherwise the updated states would no longer satisfy $|\bar{\xi}_i\rangle = \hat{T}|\xi_i\rangle$ and the exact Kramers degeneracy would be spuriously broken.

In practice, we work with a 4×4 Jacobi matrix that is block-diagonal in the ordered basis (i, j, \bar{i}, \bar{j}) ,

$$\mathbf{Q}_m(\gamma, \phi) = \begin{bmatrix} \cos \gamma & -\sin \gamma e^{-i\phi} & 0 & 0 \\ \sin \gamma e^{i\phi} & \cos \gamma & 0 & 0 \\ 0 & 0 & \cos \gamma & -\sin \gamma e^{i\phi} \\ 0 & 0 & \sin \gamma e^{-i\phi} & \cos \gamma \end{bmatrix}, \quad (17)$$

where the upper-left block mixes (i, j) and the lower-right block mixes their time-reversal partners (\bar{i}, \bar{j}) with the conjugate phase.

3.3 Solving for optimal rotation matrix

Finally, for both the dipole and spin diabatization steps, we note that the 2×2 or 4×4 rotational steps involve complex-valued matrices (Eq. 16 and 17, respectively) for which the solutions in Ref. 44 are not immediately applicable. Nevertheless, the solutions γ and ϕ for each Jacobi matrix \mathbf{Q}_m can be obtained by solving a cubic equation that maximizes the corresponding localization functional. See Supporting Information (Sec. 7) for more details.

Below, as an example, we will focus on a pair of two Kramers pairs, together with the TRS constraints above. For such a problem, we require only three (rather than $4 \times \frac{3}{2} = 6$) independent 4×4 rotations coupling (i, j) , (i, \bar{j}) , and (j, \bar{i}) in the dipole. Note that, without TRS, for a generic four-state problem, we would require $n(n-1)/2 = 6$ independent distinct pairwise rotations. Thereafter, in line with Sec. 3.1 above, after we localize the charges, we

calculate two independent 2×2 rotations within the (i, \bar{i}) and (j, \bar{j}) subspaces so as to localize the spin.

4 Numerical Results

We consider an open-shell system with an odd number of electrons undergoing charge transfer in presence of SOC. As an illustrative example, we focus on the phenoxy-phenol (ph-ph) system, in which charge is transferred between two phenyl fragments as the bridging hydrogen atom moves from one fragment to the other (See Fig. 1 (A)). The electronic structure for this CT process can be described in terms of two adiabatic states, which in absence of any external magnetic field, are doubly degenerate by the Kramers theorem. The present study builds on Paper 1, where the two lowest adiabatic doublets were analyzed in detail using Dynamically-weighted State-Averaged Constrained CASSCF (eDSC/hDSC) which is generalized to include complex-valued orbitals. We have implemented the energy calculations and diabatization algorithm in a development version of Q-Chem.⁴⁹ This phenoxy-phenol(ph-ph) system has been studied before within a restricted open-shell framework^{50,51} and the adiabatic states are the same as obtained in Paper 1.

4.1 Diabatic states

As shown in Fig. 2, the diabatization procedure described above yields smooth, physically meaningful potential energy surfaces that exhibit well-defined crossings. To assess the robustness of the diabatization scheme, we applied the latter to the large range of spin-orbit coupling (SOC) strengths explored in Paper I. As shown in Fig. 3, the resulting diabatic potential energy surfaces remain smooth and exhibit consistent crossing behavior over the entire range of SOC scaling factor (η). Fig. 4 compares the active-space electron densities of the two charge-transfer diabatic states at three representative geometries for η values 1 and 200. For both SOC strengths, each diabat exhibits qualitatively distinct left- vs right-

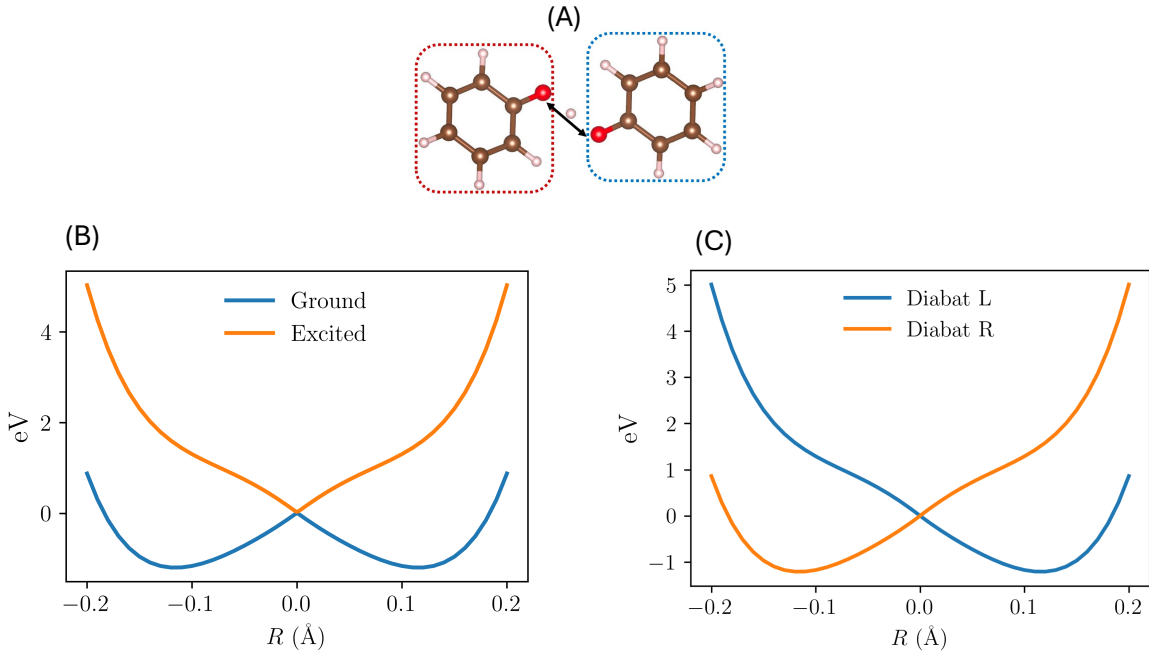


Figure 2: Potential energy curves for charge transfer along the reaction coordinate R corresponding to a proton coupled electron transfer for a phenoxy-phenol (ph-ph) complex. (A) A visualization of the system whereby the bridging hydrogen is transfers between the two symmetrically located fragments. The internuclear distance between oxygen atoms is 2.459 Å. The numerical value on the x-axis represents the displacement of the hydrogen from the midpoint between the two oxygens. (B) Adiabatic surfaces. (C) The left (L) and right (R) diabatic surfaces. The charge transfer diabatic states are doubly degenerate (just like the adiabatic states).

localized density. At strong SOC, the electron density varies more noticeably with geometry, indicating stronger mixing of orbital character along the reaction coordinate.

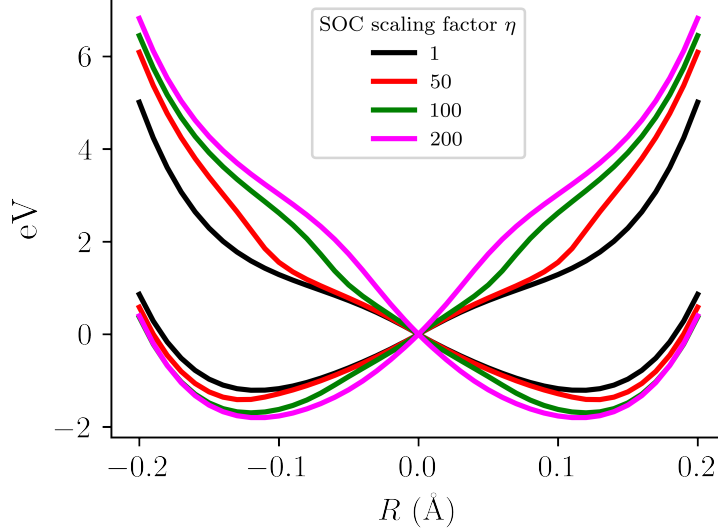


Figure 3: Diabatic PESs for different SOC values with scaling factor $\eta = [1, 50, 100, 200]$. Details about the form of spin-orbit coupling are in Paper 1. Note that increasing the SOC can drastically change the surfaces.

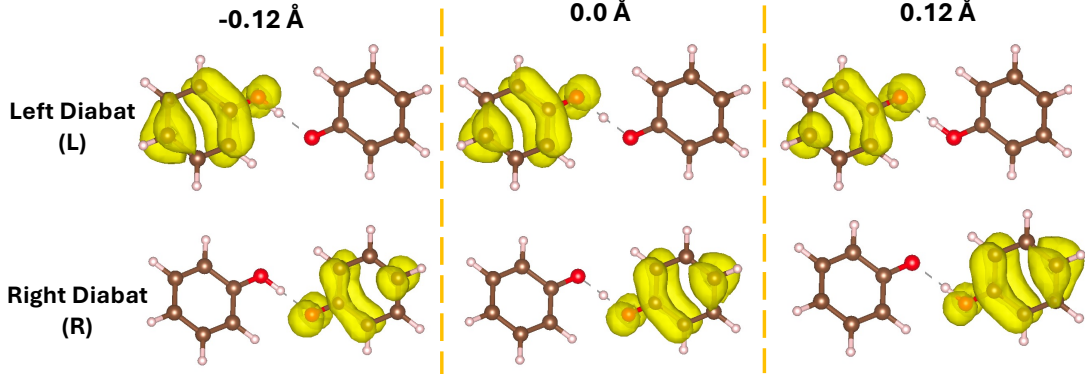
4.2 Spin expectation values and pseudospin texture

Next, for each diabatic state along the reaction coordinate, we compute the spin expectation vector

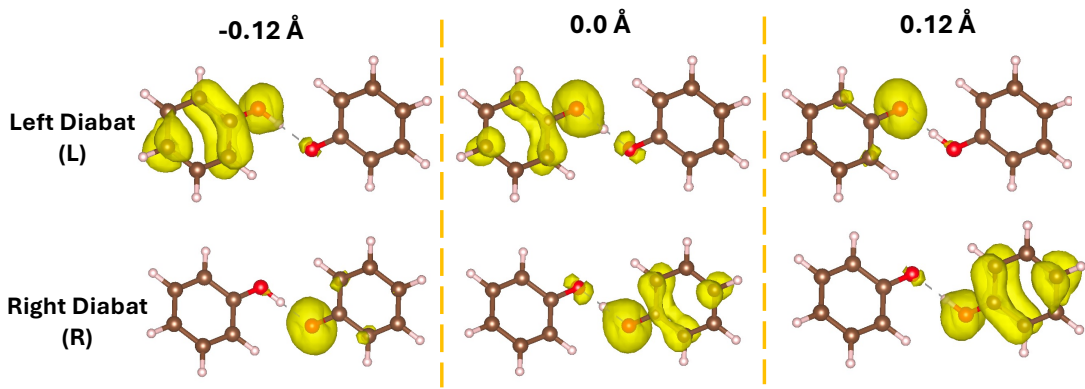
$$\mathbf{s}(\mathbf{R}) = (\langle \hat{S}_x \rangle, \langle \hat{S}_y \rangle, \langle \hat{S}_z \rangle), \quad \langle \hat{S}_\alpha \rangle = \langle \xi(\mathbf{R}) | \hat{S}_\alpha | \xi(\mathbf{R}) \rangle. \quad (18)$$

Note that the diabatic states are defined as unitary rotations within the projected space spanning two Kramers doublets. Therefore, spin expectation values of diabatic states are projected observables, i.e., *effective-spin* or *pseudospin* in the sense of the Kramers-doublet literature.^{52,53}

Figure 5 compares the Cartesian components of $\mathbf{s}(\mathbf{R})$ for weak ($\eta = 1$) and strong ($\eta = 200$) SOC strength, shown for the two localized diabats (L and R); for a definition of the xyz directions, see Fig. 6. In this diabatic basis, the spin expectation values vary smoothly with geometry, consistent with the intended charge-spin localization within the chosen four-state adiabatic basis. Because each Kramers doublet carries an intrinsic SU(2)



(A) Active orbital electron density with SOC strength $\eta = 1$.



(B) Active orbital electron density with SOC strength $\eta = 200$.

Figure 4: A comparison of the active orbital electron densities for two charge transfer diabatic states at different SOC coupling strengths. Plotted at $R = [-0.12 \text{ \AA}, 0.0 \text{ \AA}, 0.12 \text{ \AA}]$

gauge freedom, the Cartesian components $\langle \hat{S}_\alpha \rangle$ would normally exhibit spurious, rapidly varying fluctuations under different—yet physically equivalent—choices of gauge within the doublet. Our localized diabatic gauge fixes this rapidly varying gauge, leading to the smooth, slowly varying behavior. Additionally, time-reversal symmetry is preserved in our diabatic representation, i.e., for each diabat the spin expectation values are equal in magnitude and opposite in sign for the time-reversal partners.

While Fig. 5 reports the component-wise evolution of the spin expectation vector in Eq. 18, it is often more informative to quantify how the *direction* of $\mathbf{s}(\mathbf{R})$ rotates along the reaction coordinate, i.e., the emergence of a pseudospin texture in configuration space. Specifically, we let the position of bridging hydrogen vary and we choose a viewing axis $\hat{\mathbf{w}}$

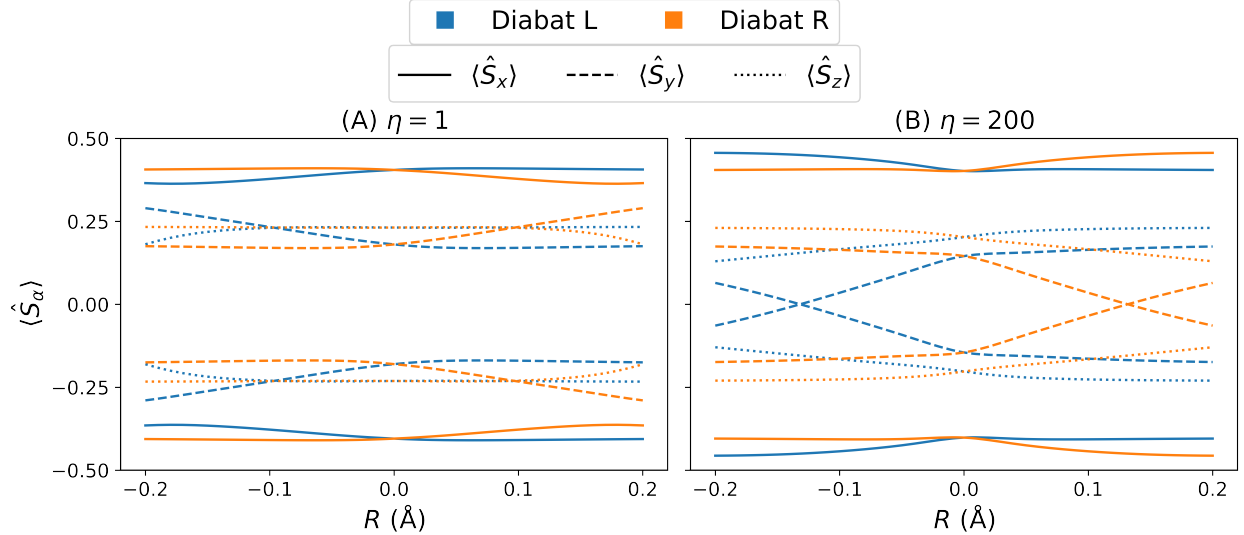


Figure 5: Spin expectation values $\langle \hat{S}_\alpha \rangle$ ($\alpha = x, y, z$) along the reaction coordinate for SOC strengths (A) $\eta = 1$ and (B) $\eta = 200$. Diabats L and R are shown in blue and orange, respectively. Solid, dashed, and dotted lines denote $\langle \hat{S}_x \rangle$, $\langle \hat{S}_y \rangle$, and $\langle \hat{S}_z \rangle$. For each diabat, the two time-reversal partners exhibit equal-and-opposite spin expectation values. See Fig. 6 for a definition of the xyz axes.

(here the O–O internuclear axis between two oxygen in Fig. 6) and remove the component of $\mathbf{s}(\mathbf{R})$ parallel to $\hat{\mathbf{w}}$,

$$\mathbf{s}_\perp(\mathbf{R}) = \mathbf{s}(\mathbf{R}) - (\mathbf{s}(\mathbf{R}) \cdot \hat{\mathbf{w}}) \hat{\mathbf{w}}, \quad \hat{\mathbf{u}}(\mathbf{R}) = \frac{\mathbf{s}_\perp(\mathbf{R})}{\|\mathbf{s}_\perp(\mathbf{R})\|}, \quad (19)$$

so that $\hat{\mathbf{u}}(\mathbf{R})$ is a unit vector lying in the plane perpendicular to $\hat{\mathbf{w}}$. We then compute the relative signed angle between $\hat{\mathbf{u}}(\mathbf{R}_{\text{ref}})$ and $\hat{\mathbf{u}}(\mathbf{R})$ using a smooth arctan convention (atan2 by C++),

$$\theta(\mathbf{R}) = \text{atan2}\left(\hat{\mathbf{w}} \cdot (\hat{\mathbf{u}}(\mathbf{R}_{\text{ref}}) \times \hat{\mathbf{u}}(\mathbf{R})), \hat{\mathbf{u}}(\mathbf{R}_{\text{ref}}) \cdot \hat{\mathbf{u}}(\mathbf{R})\right), \quad (20)$$

which returns a signed rotation relative to the reference geometry at \mathbf{R}_{ref} . The sign is fixed by the right-hand rule about $\hat{\mathbf{w}}$, allowing clockwise and anticlockwise rotations to be distinguished. Figure 7 uses the signed angle $\theta(\mathbf{R})$ to quantify, for both weak and strong SOC, how the pseudospin quantization axis rotates as the molecule progresses along the

reaction coordinate.

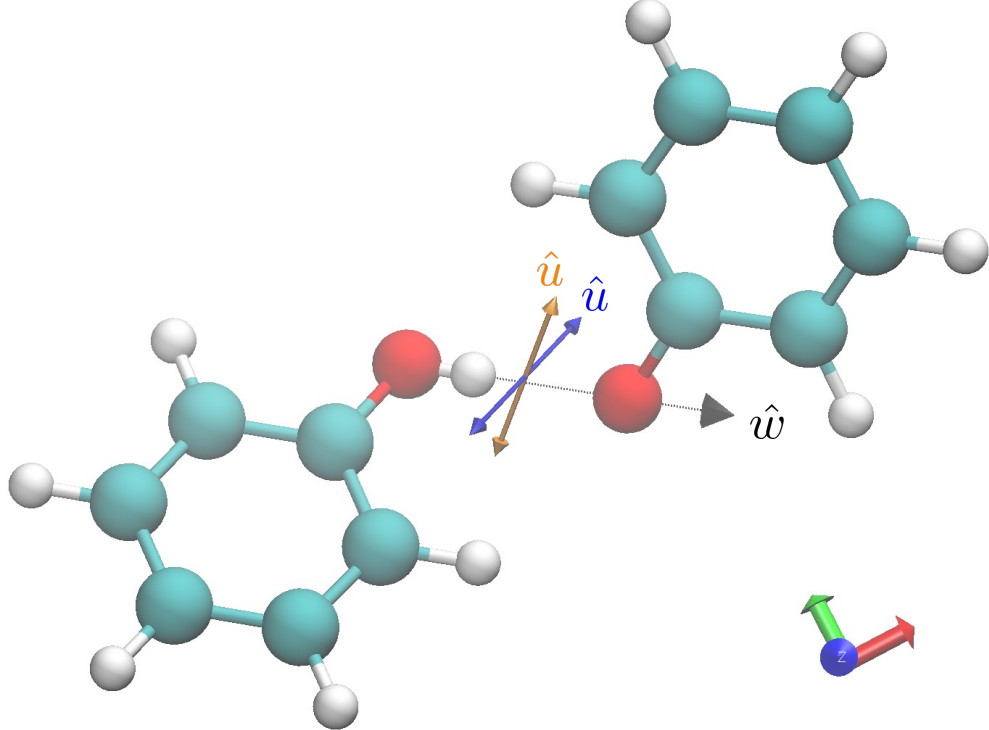


Figure 6: A visualization of the PCET process in phenoxy-phenol system, where hydrogen transfers between (red) oxygen fragments; the direction of hydrogen transfer defines the \hat{w} direction along the reaction coordinate. The blue and orange arrows (labelled \hat{u}) are defined by spin expectation values in the body frame for the Left(L) and Right(R) diabats, respectively. See Eq. 19 for the relation between these vectors. The body frame directions are defined in bottom right with Z-axis coming out of the plane formed by red (X) and green (Y) arrows. The Cartesian coordinates are provided in Supplementary Information of Paper 1.

Overall, note that the diabatization procedure from Sec. 3 is able to reproduce a smooth and reasonably slowly changing spin axis as a function of nuclear position, offering us a reasonable starting frame for modeling spin effects during electron transfer (with minimal derivative couplings induced between different spin directions).

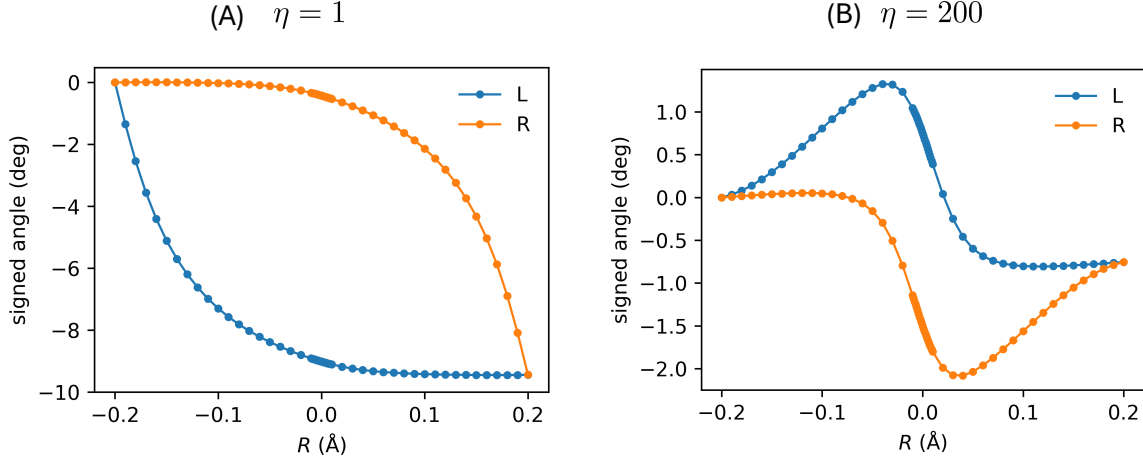


Figure 7: Signed angle $\theta(\mathbf{R})$ with reference spin vector chosen at $\mathbf{R}_{\text{ref}} = -0.2 \text{ \AA}$ geometry. Each point shows the signed rotation of the projected pseudospin direction relative to \mathbf{R}_{ref} , where pseudospins are projected into the plane perpendicular to the reaction coordinate. (A) $\eta = 1$ and (B) $\eta = 200$.

5 Discussion

5.1 Spin symmetry vs time-reversal symmetry

Although they are often conflated, for the current manuscript, it is crucial to distinguish spin-rotation symmetry from time-reversal symmetry (TRS). In the absence of external magnetic fields, TRS arises because $[\hat{H}, \hat{T}] = 0$ where T is the anti-linear time-reversal operator. For odd-electron (half-integer) systems, $\hat{T}^2 = -1$ and TRS implies Kramers degeneracy. By contrast, “spin symmetry” arises for Hamiltonians that satisfy $[\hat{H}, \hat{S}_x] = [\hat{H}, \hat{S}_y] = [\hat{H}, \hat{S}_z] = 0 = [\hat{H}, \hat{S}^2] = 0$, leading to a global SU(2) spin-rotation invariance generated by \hat{S} . These two symmetries are independent: spin-symmetry need not imply TRS and TRS need not imply spin symmetry or conservation of \hat{S} . In particular, when SOC is present, TRS is unchanged but $[\hat{H}, \hat{S}^2] \neq 0$ and $[\hat{H}, \hat{S}] \neq 0$. Thus, by calculating the expectation value of \hat{S}^2 , we can learn about how strongly spin-symmetry is broken by the presence of SOC. Note that, without any SOC, one should always recover $\langle S^2 \rangle = 3/4$ for a doublet, and any deviation from this value is the result of spin contamination.

Within the realm of standard (variational) electronic structure calculations,^{54–57} one of-

ten faces a trade-off: enforcing the exact symmetries of the electronic Hamiltonian yields symmetry-adapted yet high energy solutions, whereas relaxing such constraints often gives a lower energy yet symmetry broken state with unphysical quantum numbers (e.g., spin contamination); this tradeoff is termed Löwdin’s “symmetry dilemma”.⁵⁸ Note that, for the method described in Paper I, there is no spin contamination in the absence of SOC; deviations from $\langle \hat{S}^2 \rangle = 3/4$ arise only when SOC is included.

5.2 $\langle \hat{S}^2 \rangle$ along a reaction coordinate

With the background above in mind, we have analyzed $\langle \hat{S}^2 \rangle$ values across the reaction coordinate. As established in Ref. 59, for a single Slater determinant based on Generalized Hartree-Fock (GHF) wavefunction, the expectation value of \hat{S}^2 is:

$$\begin{aligned} \langle \psi_i | \hat{S}^2 | \psi_i \rangle &= \left(\frac{N_\alpha}{2} - \frac{N_\beta}{2} \right) \left(\frac{N_\alpha}{2} - \frac{N_\beta}{2} + 1 \right) + \frac{1}{4} \left(N_e - \sum_{i,j=1}^{N_e} |\langle \psi_{i\alpha} | \psi_{j\alpha} \rangle - \langle \psi_{i\beta} | \psi_{j\beta} \rangle|^2 \right) \\ &\quad + \left(N_\beta - \sum_{i,j=1}^{N_e} \langle \psi_{i\alpha} | \psi_{j\beta} \rangle \langle \psi_{j\beta} | \psi_{i\alpha} \rangle \right) + \left| \sum_{i=1}^{N_e} \langle \psi_{i\beta} | \psi_{i\alpha} \rangle \right|^2, \end{aligned} \quad (21)$$

where each GHF spin-orbital is a two-component spinor

$$|\psi_i\rangle \equiv \begin{pmatrix} |\psi_{i\alpha}\rangle \\ |\psi_{i\beta}\rangle \end{pmatrix}. \quad (22)$$

Eq. 21 has been derived in detail in Ref. 59 and decomposes the GHF spin expectation value into four distinct contributions. In particular, the first term is analogous to Restricted Open-Shell Hartree-Fock (ROHF) expression where the “number of α -spin electrons” (respectively “number of β -spin electrons”) are defined as

$$N_\alpha := \sum_{i=1}^{N_e} \langle \psi_{i\alpha} | \psi_{i\alpha} \rangle \quad (\text{respectively, } N_\beta := \sum_{i=1}^{N_e} \langle \psi_{i\beta} | \psi_{i\beta} \rangle) \quad (23)$$

where $N_e = N_\alpha + N_\beta$ is the total number of electrons.

We analyze the deviation of $\langle \hat{S}^2 \rangle$ from the expected value of 0.75 in Fig. 8. We find two conclusions. First, note the scale on the y-axis of Fig. 8 (A) which plots the deviations before and after dipole diabatization (subsequent spin diabatization does not alter this value). Clearly, with minimal SOC ($\eta = 10$), $\langle \hat{S}^2 \rangle$ of the resulting ground state changes by only $0.05\% = 0.003/0.75$. Second, when the states cross at $R = 0.0 \text{ \AA}$, we find only a very small change in $\langle \hat{S}^2 \rangle$ between diabat and adiabat, with a relative change of $0.00002/0.00320 = 0.006\%$. In Panel (B), we plot the deviation at diabatic crossing for different SOC strength. We find that, although the total $\langle \hat{S}^2 \rangle$ value strongly changes with SOC, the diabatic and adiabatic states have very similar $\langle \hat{S}^2 \rangle$ values themselves. For a general comparison, the $\langle \hat{S}^2 \rangle$ value (at diabatic crossing) for a UHF calculation even without SOC is 1.475, a significant deviation of more than 96 %, arising from the spin contamination.

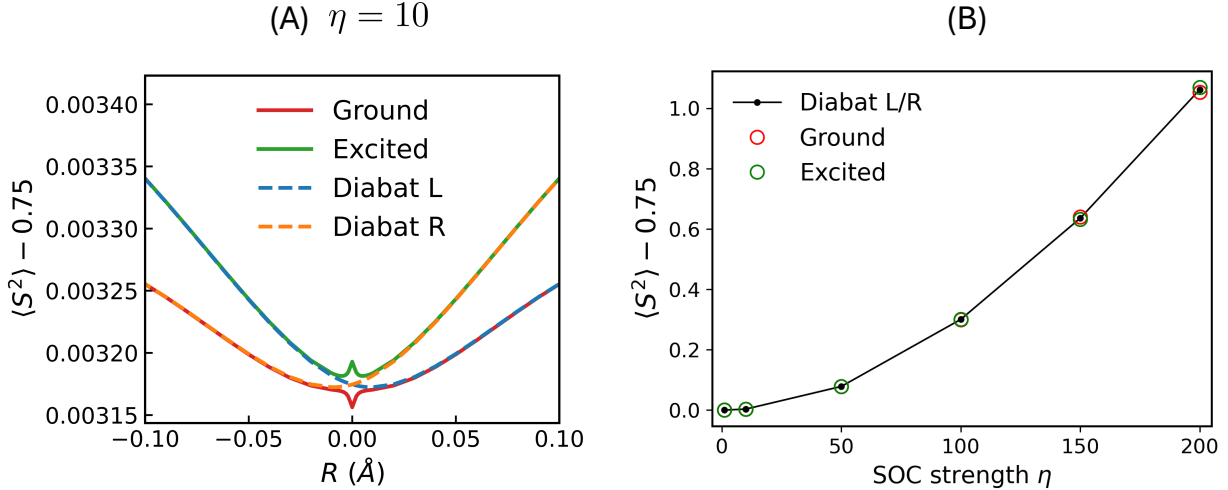


Figure 8: The deviation in $\langle \hat{S}^2 \rangle$ value from 0.75. (A) Deviation for SOC strength $\eta = 10$ along the reaction coordinate. Here, we plot the values for both adiabatic and diabatic curves. (B) The deviation in the expectation value as a function of SOC strength η for diabatic states at the central geometry ($R = 0.0 \text{ \AA}$) where the diabats cross.

6 Conclusion

We have developed and implemented a unified framework for constructing diabatic states that are simultaneously localized in both charge and spin for open-shell molecular systems subject to spin-orbit coupling. By combining dipole- and spin-based localization criteria within a sequence of complex-unitary Jacobi sweeps, the method achieves smooth potential energy surfaces that maintain Kramers degeneracy and preserve key symmetry properties. Moreover, our diabatization framework provides a physical picture in which spin localization is understood as aligning the spin-quantization axis (pseudospin) smoothly and as steadily as possible along the reaction coordinate.

The most crucial next question of this research direction is: what are the implications of this changing spin as far as electron transfer is concerned. In particular, there is a growing consensus that, in chiral environments, electron transfer can have a spin preference, resulting in so-called “chiral induced spin selectivity.”¹⁰ To that end, one would very much like to explore how the “chirality of the reaction path” affects rotations in the pseudo-spin axis. And given that any changes in the pseudospin-axis must originate from SOC, can we correlate such changes with orbital helicity^{60,61} and what are the consequences for charge-transfer reactions?

Finally, perhaps most interestingly, in order to more deeply probe CISS, one would like to explore the diabatic states described above in the context of an external magnetic field which may well lead to a spin preference for ET. In addition, recent explorations of phase space electronic structure theory^{62–64} have indicated that one can gain additional accuracy in modeling nuclear-electronic correlation by using a zeroth order electronic Hamiltonian that depends on both nuclear position R and nuclear momentum P , and thus includes an internal magnetic field. The diabatic state basis above would appear to be an obvious starting point for more deeply exploring CISS within such a phase space framework.

7 Supplementary Information

7.1 Kramers Doublet and Pseudospin

In open-shell systems with an unpaired electron, the low-lying electronic states are typically doublets that occur as Kramers pairs. In the absence of SOC, these states are spin-pure: each can be described as either spin-up or spin-down along a fixed quantization axis, and the total spin is conserved. Upon inclusion of SOC, however, the spin and orbital degrees of freedom become entangled. The spin expectation value acquires a geometry-dependent orientation, and each adiabatic state acquires a mixed spin character. Consequently, the two members of a Kramers pair are no longer simple spin-up/spin-down partners but orthonormal states whose local spin quantization axis rotates with molecular geometry. This loss of a globally conserved spin direction complicates the description of charge localization and nonadiabatic couplings and motivates the development of a diabatic framework that can smoothly maintain both charge and spin continuity along nuclear coordinates.

Within any such two-dimensional Kramers subspace, there is no unique choice of basis. If $\{|\psi_k\rangle, |\bar{\psi}_k\rangle\}$ is one orthonormal pair, then any other orthonormal pair $\{|\psi'_k\rangle, |\bar{\psi}'_k\rangle\}$ spanning the same subspace is related by a 2×2 unitary transformation with unit determinant,

$$\begin{pmatrix} |\psi'_k\rangle \\ |\bar{\psi}'_k\rangle \end{pmatrix} = \mathbf{U} \begin{pmatrix} |\psi_k\rangle \\ |\bar{\psi}_k\rangle \end{pmatrix}, \quad \mathbf{U} \in \text{SU}(2). \quad (24)$$

This internal SU(2) freedom reflects the fact that a Kramers doublet behaves as an effective pseudospin- $\frac{1}{2}$, whose state can be represented as a point on a three-dimensional Bloch sphere (qubit). Any orthonormal basis chosen within the doublet is equivalent to selecting a particular spin-quantization axis, along which the two members of the Kramers pair carry opposite spin- $\frac{1}{2}$ projections. A rotation of pseudospin axis associated with the doublet leaves all time-reversal invariant scalar quantities (like energies) unchanged, but changes the local spin expectation value for different directions.

7.2 Jacobi sweeps

Given $N(N > 1)$ Hermitian operators $\mathbf{O}^{(k)}$ and an orthonormal basis $\{\psi_i\}$, we want to find the maximum of the functional

$$f(U) = \sum_i \sum_k (\langle \xi_i | \mathbf{O}^{(k)} | \xi_i \rangle)^2 \quad (25)$$

where

$$|\xi_j\rangle = \sum_i |\psi_i\rangle U_{ij} \quad (26)$$

and \mathbf{U} is a unitary matrix. In this work, $\mathbf{O}^{(k)}$ represents the set $\{\boldsymbol{\mu}_x, \boldsymbol{\mu}_y, \boldsymbol{\mu}_z\}$ and $\{\mathbf{S}_x, \mathbf{S}_y, \mathbf{S}_z\}$ for dipole and spin diabatization, respectively.

Numerically this optimization task can be done by successive Jacobi rotations between a pair of states using matrix \mathbf{U} . An iteration over all pairs is called a Jacobi sweep. We iterate until convergence of the maximization function in Eq. 25.

Let us now focus on a single Jacobi rotation step. Consider a 2-by-2 rotation within the subspace formed by $\{\xi_i, \xi_j\}$

$$\begin{bmatrix} \xi'_i & \xi'_j \end{bmatrix} = \begin{bmatrix} \xi_i & \xi_j \end{bmatrix} \begin{bmatrix} \cos \gamma & -\sin \gamma e^{-i\phi} \\ \sin \gamma e^{i\phi} & \cos \gamma \end{bmatrix} \quad (27)$$

For each operator $\mathbf{O}^{(k)}$, the change of Eq. 25 from this rotation is

$$\begin{aligned} \Delta f^{(k)} = & \left[O_{ii}^{(k)} \cos^2 \gamma + O_{jj}^{(k)} \sin^2 \gamma + \left(O_{ij}^{(k)} e^{i\phi} + O_{ji}^{(k)} e^{-i\phi} \right) \cos \gamma \sin \gamma \right]^2 \\ & + \left[O_{ii}^{(k)} \sin^2 \gamma + O_{jj}^{(k)} \cos^2 \gamma - \left(O_{ij}^{(k)} e^{i\phi} + O_{ji}^{(k)} e^{-i\phi} \right) \cos \gamma \sin \gamma \right]^2 - (O_{ii}^{(k)})^2 - (O_{jj}^{(k)})^2 \end{aligned} \quad (28)$$

Defining

$$A \equiv \sum_k \left[\left(\frac{O_{ij}^{(k)} e^{i\phi} + O_{ji}^{(k)} e^{-i\phi}}{2} \right)^2 - \left(\frac{O_{ii}^{(k)} - O_{jj}^{(k)}}{2} \right)^2 \right] \quad (29)$$

$$B \equiv \sum_k \frac{O_{ij}^{(k)} e^{i\phi} + O_{ji}^{(k)} e^{-i\phi}}{2} (O_{ii}^{(k)} - O_{jj}^{(k)}) \quad (30)$$

Then total change of Eq. 25 from this rotation is

$$\Delta f = \sum_k \Delta f^{(k)} = A - A \cos 4\gamma + B \sin 4\gamma = A + \sqrt{A^2 + B^2} \cos 4(\gamma - \alpha) \quad (31)$$

where

$$\cos 4\alpha = -A/\sqrt{A^2 + B^2} \quad (32)$$

$$\sin 4\alpha = B/\sqrt{A^2 + B^2} \quad (33)$$

for the real case (where $\phi \equiv 0$) the maximum is readily obtained by choosing $\gamma = \alpha + n\pi/2$ where n is an arbitrary integer. For the complex case, one needs to first maximize $A + \sqrt{A^2 + B^2}$ with respect to ϕ .

To maximize $A + \sqrt{A^2 + B^2}$, we first rewrite A and B :

$$\begin{aligned} A &= \frac{1}{4} \sum_k \left[(O_{ij}^{(k)})^2 e^{2i\phi} + (O_{ji}^{(k)})^2 e^{-2i\phi} + 2O_{ij}^{(k)} O_{ji}^{(k)} - (O_{ii}^{(k)} - O_{jj}^{(k)})^2 \right] \\ &= \frac{1}{4} \left[e^{2i\phi} \sum_k (O_{ij}^{(k)})^2 + \text{c.c.} \right] + \sum_k \left[\frac{1}{2} O_{ij}^{(k)} O_{ji}^{(k)} - \frac{1}{4} (O_{ii}^{(k)} - O_{jj}^{(k)})^2 \right] \\ &\equiv ue^{2i\phi} + u^* e^{-2i\phi} + A_0 \end{aligned} \quad (34)$$

$$\begin{aligned} B &= \frac{1}{2} \left[e^{i\phi} \sum_k O_{ij}^{(k)} (O_{ii}^{(k)} - O_{jj}^{(k)}) + \text{c.c.} \right] \\ &\equiv ve^{i\phi} + v^* e^{-i\phi} \end{aligned} \quad (35)$$

where

$$u \equiv \frac{1}{4} \sum_k (O_{ij}^{(k)})^2 \quad (36)$$

$$v \equiv \frac{1}{2} \sum_k O_{ij}^{(k)} (O_{ii}^{(k)} - O_{jj}^{(k)}) \quad (37)$$

$$A_0 \equiv \sum_k \left[\frac{1}{2} O_{ij}^{(k)} O_{ji}^{(k)} - \frac{1}{4} (O_{ii}^{(k)} - O_{jj}^{(k)})^2 \right] \quad (38)$$

u and v in general are complex numbers, and A_0, A and B are real. The ϕ that maximizes $A + \sqrt{A^2 + B^2}$ can be solved by the following equation:

$$\begin{aligned} \frac{d}{d\phi} \left(A + \sqrt{A^2 + B^2} \right) &= 0 \\ \implies -\sqrt{A^2 + B^2} \frac{dA}{d\phi} &= A \frac{dA}{d\phi} + B \frac{dB}{d\phi} \\ \implies B^2 \left[\left(\frac{dA}{d\phi} \right)^2 - \left(\frac{dB}{d\phi} \right)^2 \right] &= 2AB \frac{dA}{d\phi} \frac{dB}{d\phi} \\ \implies B \left[\left(\frac{dA}{d\phi} \right)^2 - \left(\frac{dB}{d\phi} \right)^2 \right] &= 2A \frac{dA}{d\phi} \frac{dB}{d\phi} \end{aligned} \quad (39)$$

where we've assumed $B \neq 0$.

Before we plug Eqs. 34 and 35 into Eq. 39, it's helpful to define a few notations to make the expression looks simpler. Let

$$x \equiv ue^{2i\phi} \quad (40)$$

$$y \equiv ve^{i\phi} \quad (41)$$

then

$$A = x + x^* + A_0 \quad (42)$$

$$B = y + y^* \quad (43)$$

$$\frac{dA}{d\phi} = 2i(ue^{2i\phi} - u^*e^{-2i\phi}) = 2i(x - x^*) \quad (44)$$

$$\frac{dB}{d\phi} = i(v e^{i\phi} - v^* e^{-i\phi}) = i(y - y^*) \quad (45)$$

Plugging Eqs. 42-45 into Eq. 39, and if we rewrite x and y in terms of u, v and $e^{i\phi}$, we obtain an equation for $e^{i\phi}$,

$$\alpha e^{3i\phi} + \beta e^{i\phi} + \beta^* e^{-i\phi} + \alpha^* e^{-3i\phi} = 0 \quad (46)$$

where

$$\alpha \equiv v^3 + 4A_0uv - 8u^2v^* \quad (47)$$

$$\beta \equiv -v^2v^* - 4A_0uv^* + 8uu^*v \quad (48)$$

Note that, in terms of the power of $e^{i\phi}$, this equation contains only $e^{3i\phi}, e^{i\phi}, e^{-i\phi}$ and $e^{-3i\phi}$. Moreover, the coefficient of $e^{-3i\phi}$ is the complex conjugate of the coefficient of $e^{3i\phi}$; so does the relation between $e^{i\phi}$ and $e^{-i\phi}$. One way to look at Eq. 46 is to combine the complex conjugated terms:

$$\begin{aligned} \operatorname{Re}\{\alpha e^{3i\phi}\} + \operatorname{Re}\{\beta e^{i\phi}\} &= 0 \\ \implies |\alpha| \cos(3\phi + \phi_\alpha) + |\beta| \cos(\phi + \phi_\beta) &= 0 \\ \implies \frac{\cos(3\phi + \phi_\alpha)}{\cos(\phi + \phi_\beta)} &= -\left|\frac{\beta}{\alpha}\right| \end{aligned} \quad (49)$$

Another way to look at Eq. 46 is to convert it to a cubic equation

$$\alpha\omega^3 + \beta\omega^2 + \beta^*\omega + \alpha^* = 0 \quad (50)$$

where

$$\omega \equiv e^{2i\phi} \quad (51)$$

Finally, for each Jacobi rotation, we plug in all three roots back in Eq. 25 and pick the one which gives maximum value of the optimizing functional.

8 Acknowledgments

We thank Brian Conrad and Keith Conrad for helpful discussions regarding Eq. 46. This work was supported by the National Science Foundation Grant CHE-2422858.

References

- (1) Wasielewski, M. R. Photoinduced electron transfer in supramolecular systems for artificial photosynthesis. *Chemical reviews* **1992**, *92*, 435–461.
- (2) Rochaix, J.-D. Regulation of photosynthetic electron transport. *Biochimica et Biophysica Acta (BBA)-Bioenergetics* **2011**, *1807*, 375–383.
- (3) Gust, D.; Moore, T. A.; Moore, A. L. Mimicking photosynthetic solar energy transduction. *Accounts of Chemical Research* **2001**, *34*, 40–48.
- (4) Coropceanu, V.; Chen, X.-K.; Wang, T.; Zheng, Z.; Brédas, J.-L. Charge-transfer electronic states in organic solar cells. *Nature Reviews Materials* **2019**, *4*, 689–707.

(5) Ostroverkhova, O. Organic optoelectronic materials: mechanisms and applications. *Chemical reviews* **2016**, *116*, 13279–13412.

(6) May, A. M.; Dempsey, J. L. A new era of LMCT: leveraging ligand-to-metal charge transfer excited states for photochemical reactions. *Chemical Science* **2024**, *15*, 6661–6678.

(7) Zobel, J. P.; González, L. The quest to simulate excited-state dynamics of transition metal complexes. *JACS Au* **2021**, *1*, 1116–1140.

(8) Naaman, R.; Paltiel, Y.; Waldeck, D. H. Chiral molecules and the electron spin. *Nature Reviews Chemistry* **2019**, *3*, 250–260.

(9) Eckvahl, H. J.; Tcyru nikov, N. A.; Chiesa, A.; Bradley, J. M.; Young, R. M.; Carretta, S.; Krzyaniak, M. D.; Wasielewski, M. R. Direct observation of chirality-induced spin selectivity in electron donor–acceptor molecules. *Science* **2023**, *382*, 197–201.

(10) Naaman, R.; Waldeck, D. H. What Can CISS Teach Us about Electron Transfer? *The Journal of Physical Chemistry Letters* **2024**, *15*, 11002–11006.

(11) Newton, M. D.; Sutin, N. Electron transfer reactions in condensed phases. *Annu. Rev. Phys. Chem.;(United States)* **1983**, *35*.

(12) Marcus, R. A.; Sutin, N. Electron Transfers in Chemistry and Biology. *Biochimica et Biophysica Acta* **1985**, *811*, 265–322.

(13) Wörner, H. J.; Arrell, C. A.; Banerji, N.; Cannizzo, A.; Chergui, M.; Das, A. K.; Hamm, P.; Keller, U.; Kraus, P. M.; Liberatore, E.; others Charge migration and charge transfer in molecular systems. *Structural dynamics* **2017**, *4*.

(14) Marchi, M.; Gehlen, J. N.; Chandler, D.; Newton, M. Diabatic surfaces and the pathway for primary electron transfer in a photosynthetic reaction center. *Journal of the American Chemical Society* **1993**, *115*, 4178–4190.

(15) Hsu, C.-P.; Marcus, R. A sequential formula for electronic coupling in long range bridge-assisted electron transfer: Formulation of theory and application to alkanethiol monolayers. *The Journal of chemical physics* **1997**, *106*, 584–598.

(16) Boys, S. F. Construction of Some Molecular Orbitals to Be Approximately Invariant for Changes from One Molecule to Another. *Reviews of Modern Physics* **1960**, *32*, 296–299.

(17) Foster, J. M.; Boys, S. F. Canonical Configurational Interaction Procedure. *Reviews of Modern Physics* **1960**, *32*, 300–302.

(18) Cave, R. J.; Newton, M. D. Generalization of the Mulliken-Hush treatment for the calculation of electron transfer matrix elements. *Chemical Physics Letters* **1996**, *249*, 15–19.

(19) Subotnik, J. E.; Yeganeh, S.; Cave, R. J.; Ratner, M. A. Constructing diabatic states from adiabatic states: Extending generalized Mulliken-Hush to multiple charge centers with Boys localization. *Journal of Chemical Physics* **2008**, *129*, 244101.

(20) Edmiston, C.; Ruedenberg, K. Localized atomic and molecular orbitals. *Reviews of Modern Physics* **1963**, *35*, 457.

(21) Voityuk, A. A.; Rosch, N. Fragment charge difference method for estimating donor-acceptor electronic coupling: Application to DNA π -stacks. *Journal of Chemical Physics* **2002**, *117*, 5607–5616.

(22) Voityuk, A. A. Fragment transition density method to calculate electronic coupling for excitation energy transfer. *Journal of Chemical Physics* **2014**, *140*, 244117.

(23) You, Z.; Shao, Y.; Hsu, C. P. Calculating electron transfer couplings by the spin-flip approach: energy splitting and dynamical correlation effects. *Chemical Physics Letters* **2004**, *390*, 116–123.

(24) You, Z. Q.; Hsu, C. P.; Fleming, G. Triplet-Triplet Energy-Transfer Coupling: Theory and Calculation. *Journal of Chemical Physics* **2006**, *124*, 044506.

(25) Hsu, C.-P.; You, Z.-Q.; Chen, H.-C. Characterization of the short-range couplings in excitation energy transfer. *The Journal of Physical Chemistry C* **2008**, *112*, 1204–1212.

(26) Venghaus, F.; Eisfeld, W. Block-diagonalization as a tool for the robust diabatization of high-dimensional potential energy surfaces. *The Journal of Chemical Physics* **2016**, *144*, 114110.

(27) Wittenbrink, N.; Venghaus, F.; Williams, D.; Eisfeld, W. A new approach for the development of diabatic potential energy surfaces: Hybrid block-diagonalization and diabatization by ansatz. *The Journal of Chemical Physics* **2016**, *145*.

(28) You, Z.-Q.; Hsu, C.-P. The fragment spin difference scheme for triplet-triplet energy transfer coupling. *The Journal of chemical physics* **2010**, *133*.

(29) Grofe, A.; Chen, X.; Liu, W.; Gao, J. Spin-multiplet components and energy splittings by multistate density functional theory. *The journal of physical chemistry letters* **2017**, *8*, 4838–4845.

(30) Grofe, A.; Qu, Z.; Truhlar, D. G.; Li, H.; Gao, J. Diabatic-at-construction method for diabatic and adiabatic ground and excited states based on multistate density functional theory. *Journal of chemical theory and computation* **2017**, *13*, 1176–1187.

(31) Liu, C.; Xu, Y.; Bao, P.; Lu, Y.; Gao, J. Multistate density functional theory for local and charge-transfer tripdoublet states from triplet-free radical interactions. *arXiv preprint arXiv:2503.17559* **2025**,

(32) Domcke, W.; Mishra, S.; Poluyanov, L. V. The relativistic $E \times E$ Jahn–Teller effect revisited. *Chemical physics* **2006**, *322*, 405–410.

(33) Marian, C. M. Spin-orbit coupling and intersystem crossing in molecules. *Wiley Interdisciplinary Reviews: Computational Molecular Science* **2012**, *2*, 187–203.

(34) Thorning, F.; Jensen, F.; Ogilby, P. R. Geometry dependence of spin-orbit coupling in complexes of molecular oxygen with atoms, H₂, or organic molecules. *The Journal of Physical Chemistry A* **2022**, *126*, 834–844.

(35) Zeng, T. A diabatization protocol that includes spin-orbit coupling. *The Journal of Chemical Physics* **2017**, *146*.

(36) Atchity, G. J.; Ruedenberg, K. Determination of diabatic states through enforcement of configurational uniformity. *Theoretical Chemistry Accounts* **1997**, *97*, 47–58.

(37) Nakamura, H.; Truhlar, D. G. The direct calculation of diabatic states based on configurational uniformity. *Journal of Chemical Physics* **2001**, *115*, 10353–10372.

(38) Hoyer, C. E.; Xu, X.; Ma, D.; Gagliardi, L.; Truhlar, D. G. Diabatization based on the dipole and quadrupole: The DQ method. *Journal of Chemical Physics* **2014**, *141*, 114104.

(39) Voorhis, T. V.; Kowalczyk, T.; Kaduk, B.; Wang, L. P.; Cheng, C. L.; Wu, Q. The Diabatic Picture of Electron Transfer, Reaction Barriers, and Molecular Dynamics. *Annual Reviews in Physical Chemistry* **2010**, *61*, 149–170.

(40) Shu, Y.; Varga, Z.; Kanchanakungwankul, S.; Zhang, L.; Truhlar, D. G. Diabatic states of molecules. *The Journal of Physical Chemistry A* **2022**, *126*, 992–1018.

(41) Subotnik, J. E.; Cave, R. J.; Steele, R. P.; Shenvi, N. The initial and final states of electron and energy transfer processes: diabatization as motivated by system-solvent interactions. *Journal of Chemical Physics* **2009**, *130*, 234102.

(42) Marcus, R. A. On the Theory of Oxidation-Reduction Reactions Involving Electron Transfer. I. *Journal of Chemical Physics* **1956**, *24*, 966–978.

(43) Subotnik, J. E.; Alguire, E. C.; Ou, Q.; Landry, B. R.; Fatehi, S. The Requisite Electronic Structure Theory To Describe Photoexcited Nonadiabatic Dynamics: Nonadiabatic Derivative Couplings and Diabatic Electronic Couplings. *Accounts of Chemical Research* **2015**, *48*, 1340–1350.

(44) Edmiston, C.; Ruedenberg, K. Localized Atomic and Molecular Orbitals. *Reviews of Modern Physics* **1963**, *35*, 457–464.

(45) Cardoso, J.-F.; Souloumiac, A. Jacobi angles for simultaneous diagonalization. *SIAM journal on matrix analysis and applications* **1996**, *17*, 161–164.

(46) Ciupka, J.; Hanrath, M.; Dolg, M. Localization scheme for relativistic spinors. *The Journal of chemical physics* **2011**, *135*.

(47) Alguire, E. C.; Fatehi, S.; Shao, Y.; Subotnik, J. E. An analysis of localized diabatic states beyond the Condon approximation for excitation energy transfer processes. *Journal of Physical Chemistry A* **2014**, *118*, 11891–11900.

(48) Kramers, H. A. Théorie générale de la rotation paramagnétique dans les cristaux. *Proc. Acad. Amst* **1930**, *33*.

(49) Epifanovsky, E.; Gilbert, A. T.; Feng, X.; Lee, J.; Mao, Y.; Mardirossian, N.; Pokhilko, P.; White, A. F.; Coons, M. P.; Dempwolff, A. L.; others Software for the frontiers of quantum chemistry: An overview of developments in the Q-Chem 5 package. *The Journal of chemical physics* **2021**, *155*, 084801.

(50) Qiu, T.; Bian, X.; Tao, Z.; Subotnik, J. E. A fast and smooth one-electron approach for investigating charge transfer states and D1–D0 crossings for systems with odd numbers of electrons. *The Journal of Chemical Physics* **2024**, *160*.

(51) Qiu, T.; Subotnik, J. E. An Efficient Algorithm for Constrained CASSCF (1, 2) and

CASSCF (3, 2) Simulations as Relevant to Electron and Hole Transfer Problems. *Journal of Chemical Theory and Computation* **2024**, *20*, 8960–8969.

(52) Steiner, U. E.; Serebrennikov, Y. A. Adiabatic rotation of effective spin. I. New insight into spin-rotational interaction. *The Journal of chemical physics* **1994**, *100*, 7503–7507.

(53) Chibotaru, L. F.; Ungur, L. Ab initio calculation of anisotropic magnetic properties of complexes. I. Unique definition of pseudospin Hamiltonians and their derivation. *The Journal of chemical physics* **2012**, *137*.

(54) Menon, A. S.; Radom, L. Consequences of spin contamination in unrestricted calculations on open-shell species: Effect of Hartree- Fock and Møller- Plesset contributions in hybrid and double-hybrid density functional theory approaches. *The Journal of Physical Chemistry A* **2008**, *112*, 13225–13230.

(55) Casanova, D.; Krylov, A. I. Spin-flip methods in quantum chemistry. *Physical Chemistry Chemical Physics* **2020**, *22*, 4326–4342.

(56) Bučinský, L.; Malček, M.; Biskupič, S.; Jayatilaka, D.; Buechel, G. E.; Arion, V. B. Spin contamination analogy, Kramers pairs symmetry and spin density representations at the 2-component unrestricted Hartree–Fock level of theory. *Computational and Theoretical Chemistry* **2015**, *1065*, 27–41.

(57) Kasper, J. M.; Jenkins, A. J.; Sun, S.; Li, X. Perspective on Kramers symmetry breaking and restoration in relativistic electronic structure methods for open-shell systems. *The Journal of Chemical Physics* **2020**, *153*.

(58) Lykos, P.; Pratt, G. Discussion on the Hartree-Fock approximation. *Reviews of Modern Physics* **1963**, *35*, 496.

(59) Cassam-Chenaï, P. Spin contamination and noncollinearity in general complex Hartree–Fock wave functions. *Theoretical Chemistry Accounts* **2015**, *134*, 125.

(60) Bro-Jørgensen, W.; Garner, M. H.; Solomon, G. C. Quantification of the helicity of helical molecular orbitals. *The Journal of Physical Chemistry A* **2021**, *125*, 8107–8115.

(61) Garner, M. H.; Corminboeuf, C. The fundamental relation between electrohelicity and molecular optical activity. *Physical Chemistry Chemical Physics* **2023**, *25*, 15200–15208.

(62) Bian, X.; Duston, T.; Bradbury, N.; Tao, Z.; Bhati, M.; Qiu, T.; Wu, X.; Wu, Y.; Subotnik, J. E. The phase-space way to electronic structure theory and subsequently chemical dynamics. *Chemical Physics Reviews* **2026**, *7*.

(63) Tao, Z.; Qiu, T.; Bian, X.; Duston, T.; Bradbury, N.; Subotnik, J. E. A basis-free phase space electronic Hamiltonian that recovers beyond Born–Oppenheimer electronic momentum and current density. *The Journal of Chemical Physics* **2025**, *162*.

(64) Bradbury, N. C.; Duston, T.; Tao, Z.; Rawlinson, J. I.; Littlejohn, R.; Subotnik, J. Symmetry breaking as predicted by a phase space Hamiltonian with a spin Coriolis potential. *The Journal of Chemical Physics* **2025**, *162*.